COMPARATIVE STUDY OF THE MORPHOLOGICAL, STRUCTURAL AND TEXTURAL CHARACTERISTICS OF GRAPHENE DERIVATIVES OBTAINED BY DIFFERENT OXIDATION OR REDUCTION TREATMENTS

E. Lucena-Mendoza [a, b], S. Voelger [a], G. Rodríguez [a], Y. Díaz [a], R. S. Del Toro [a*]

[a] Laboratorio de Físico Química de Superficies, Centro de Química "Dr. Gabriel Chuchani", Instituto Venezolano de Investigaciones Científicas (IVIC), Caracas 1020-A, Venezuela.
[b] Laboratorio Físico Químico, Aseguramiento de la Calidad, Planta Barquisimeto, Mondelez VZ C.A., Venezuela.

*Corresponding author, Email: raqueldeltoro.ivic@gmail.com, rdeltoro@correo.ivic.gob.ve, phone: +58 (212) 504.3082/1346, Fax.: 5041426

Received: 15-07-2024 Accepted: 12-09-2024
Published: 27-03-2025

ABSTRACT
This is a comparative study of the nature of oxygenated functional groups incorporated or removed from the graphene derivative, through different synthetic study methodologies, as well as its correlation with the crystalline/amorphous structure, morphology and porous texture generated in the synthesized material. For this purpose, three graphene oxide (GO) derivatives were synthesized by reaction of graphite with an oxidizing mixture. GO1 and GO2 were obtained using the traditional Hummers method and GO3 by a modified Hummers method, with variations in stoichiometry, temperature, and reaction time. In addition, a green synthesis of reduced graphene oxide (r-GO), starting from GO3 and L-ascorbic acid as reducing agent was investigated. The solids were characterized by FT-IR, XRD, SEM, UV-Vis and textural analysis by N_2 physisorption.

Keywords: graphene oxide, reduced graphene oxide, characterization, SEM.

ESTUDIO COMPARATIVO DE LAS CARACTERÍSTICAS MORFOLÓGICAS, ESTRUCTURALES Y TEXTURALES DE DERIVADOS DE GRAFENO OBTENIDOS POR DISTINTOS TRATAMIENTOS DE OXIDACIÓN O REDUCCIÓN

RESUMEN
El presente, es un estudio comparativo de la naturaleza de grupos funcionales oxigenados incorporados o eliminados del derivado de grafeno, a través de diferentes metodologías sintéticas de estudio, así como, su correlación con la estructura cristalina/amorfa, morfología y textura porosa generada en el material sintetizado. Para ello, se sintetizaron tres derivados de óxido de grafeno (GO) por reacción del grafito con una mezcla oxidante. Se obtuvo GO1 y GO2 empleando el método Hummers tradicional y GO3 por un método de Hummers modificado, con variaciones en estequiometría, temperatura, y tiempo de reacción. Además, se exploró una síntesis verde de óxido de grafeno reducido (r-GO), a partir de GO3 y ácido *L*-ascórbico como agente reductor. Los sólidos fueron caracterizados por FT-IR, DRX, MEB, UV-Vis y análisis textural por fisisorción de N_2.

Palabras claves: oxido de grafeno, oxido de grafeno reducido, caracterización, MEB.

INTRODUCTION

Graphene and its derivatives, in particular graphene oxide and reduced graphene oxide, are being investigated in almost all fields of science, technology, and engineering. They have been the subject of study for just over 180 years. Many methods have been proposed for the preparation of graphene and its by-products. Currently, graphene and its derivative reduced graphene oxide can be obtained by chemical manipulation of graphene oxide [1]. Since its publication in 1958, the Hummers method, which uses a series of oxidizing agents, has had a significant impact and is the most widely used experimental protocol for obtaining this carbonaceous material [2]. The resulting

GO structure may be related to the "over-oxidation" derived from the synthesis method employed. When comparing the oxidation conditions in the Hummers and Brodie methods, it is evident that both protocols with different oxidation strategies led to obtain GO with particular characteristics [3]. In this sense, the question arises about the effect of "over-oxidation" due to the synthesis method on the chemical composition, crystalline structure, and morphology of the obtained GO. In this regard, Viprya *et al.* [4] used scanning electron microscopy to characterize the morphology of GO and r-GO, in terms of the obtaining of sheets, the thickness of the edges, the contour and types of crystals formed, among others, to reveal important information related to oxygenated functional groups present. As for the chemical reduction of GO, this is carried out with conventional reducing agents such as $NaBH_4$, hydrazine or hydrazine hydrate [5]. However, the latter are highly toxic and potentially explosive, so precautions should be taken when using them in large quantities [6]. *L*-ascorbic acid (*L*-AA) as a green alternative among GO reducing agents is an inexpensive, non-toxic, and abundant substance that can reduce GO to r-GO to an acceptable level [7]. In the present study, three GO derivatives were synthesized by the reaction of graphite with an oxidizing mixture, yielding GO1 and GO2 (traditional Hummers method) and GO3 (modified Hummers method). The reduced graphene oxide r-GO3 was obtained by the reduction reaction of GO3 with *L*-ascorbic acid as a green alternative. In order to understand the modifications in composition, crystal structure, morphology and texture of the materials, the synthesized solids were characterized by FT-IR, XRD, SEM, and textural analysis by N_2 physisorption.

MATERIALS AND METHODS

Materials

All chemicals were used without further purification and purchased from commercial sources as follows: Graphite powder (Riedel-de Haën), $KMnO_4$ (99,5 %, Sigma-Aldrich), $NaNO_3$ (99 %, Merck), H_2SO_4 (98 %, Sigma-Aldrich), H_3PO_4 (85 %, Merck), H_2O_2 (30 %, Merck), EtOH (99 %, Sigma-Aldrich), HCl (37 %, Riedel-de Haën), $BaCl_2$ (99,9 %, Merck), *L*-AA (99,7 %, Riedel-de Haën).

Preparation of GO and r-GO

In order to study the effects of the preparation method on the textural, morphological and chemical properties of the obtained materials, graphene oxide was prepared by applying variations in stoichiometry, temperature and reaction time of known experimental protocols reported in the literature [2, 8, 9].

Methodology 1. Preparation of GO1 [2]

A mixture of powdered graphite (1 g) and $NaNO_3$ (0.5 g) in H_2SO_4 (23 mL) was prepared in a beaker cooled to 2 °C. $KMnO_4$ (3 g) was carefully added to the suspension while stirring vigorously. The temperature was raised to 40 °C in a controlled manner and maintained there for 6 hours with stirring. As the reaction progressed, the mixture gradually decreased in effervescence and changed to a brownish-gray color. Warm deionized (DI) water (50 mL) was then slowly added until strong effervescence and a rise in temperature occurred. The suspension, now brown in color, was stirred for 20 minutes, diluted with warm DI water (150 mL), and treated with H_2O_2 (100 mL, 3 %). This mixture was centrifuged and the supernatant was filtered resulting in a brown mass, which was washed three times with warm DI water, centrifuged, and oven-dried at 60 °C to obtain graphite oxide sheets (0.45 g). This material was then exfoliated by preparing an aqueous dispersion (1 mg/mL) under stirring for 1 h and then under ultrasound for 2 h. The dispersion was dried to obtain a powder of GO1 (0.36 g).

Methodology 2. Preparation of GO2 [2]

Powders of graphite (0.5 g), $NaNO_3$ (0.5 g) and H_2SO_4 (23 mL) were mixed and allowed to react following

Methodology 1. The brown mass collected by centrifugation was washed several times with aqueous HCl solution (5 %) and DI water. A dry material in the form of amorphous sheets was obtained, which was ground in a mortar to a fine graphite oxide powder (0.3 g), which was exfoliated to obtain GO2 (0.15 g).

Methodology 3. Preparation of GO3 [8, 9]

Firstly, powdered graphite and $KMnO_4$ were mixed in a ratio of 1:6 for 5 min and kept at 2 - 5 °C with cooling. On the other hand, a solution of H_2SO_4 and H_3PO_4 (ratio 9:1) was prepared and cooled to 2 – 5 °C. The acid solution was added to the solid mixture (graphite/$KMnO_4$) with continuous stirring until a dark green solution was obtained. This solution was heated at 65 °C for 24 h with stirring until it took on a dark purple color and was allowed to cool to 25 °C. The reaction mixture was transferred to a beaker containing 200 mL of DI water ice. H_2O_2 (70 mL) was then added with stirring to give a light brown solution. Deionized water (50 mL) was added to the solution and the precipitate was allowed to settle for 1 h. The mixture was centrifuged in batches and the supernatant was decanted to remove the metal ions in solution, obtaining a bright brown gel, which was washed successively according to the following scheme: DI water, aqueous HCl solution (30 %) to remove SO_4^{2-} ions, EtOH and again DI water, using centrifugation (7000 rpm, 30 min). The collected brown color material was dried at 50 °C for 24 h to obtain amorphous flakes which were ground to give a fine graphite oxide powder (1.3 g). For exfoliation of the material, an aqueous dispersion (0.65 mg/mL) was prepared with 1.25 g of this solid by ultrasound treatment (180 W, 60 °C, 6 h). The obtained suspension was evaporated to dryness resulting in thin films that were ground in a mortar to obtain 1.2 g of GO3 powder.

Preparation of r-GO3 [9, 10]

An aqueous suspension of GO3 (512 mL; 0.4 mg/mL) was prepared in a beaker and exfoliated by ultrasound for 1 h at 25 °C. Then an aqueous solution of *L*-AA (25 mL; 0.936 M) was slowly added and the resulting mixture was heated at 95 °C for 4 h under reflux. After cooling to 25 °C, the hydrophobic black solid deposited on the bottom of the flask was easily centrifuged to remove the supernatant, the obtained wet mass was washed with warm DI water, HCl solution (1 M), EtOH and DI water (to neutral pH) using centrifugation (7000 rpm, 20 min). The collected solid was dried in an oven at 50 ºC for 24 h, obtaining black sheets that were ground in a mortar to yield a powder of r-GO3 (150 mg).

Characterization Techniques

N_2 physisorption

The textural analysis of the synthesized materials was carried out with an automatic analyzer Micromeritics-ASAP 2010 at a temperature of 77 K. The specific surface areas were calculated by the Brunauer-Emmett-Teller (BET) method, the total pore volume (Vp) was determined by adsorption at a relative pressure of 0.98 and the pore size distribution by the Barret-Joyner-Halenda (BJH) method.

FT-IR

Infrared spectra (FT-IR) data were obtained from a Thermo Scientific Nicolet iS10 spectrometer (32 scans, between 4000-500 cm^{-1}), for this purpose each sample (0.125 wt. %) was mixed with KBr to form a pellet of 200 mg.

SEM

For the analysis of particle morphology and aggregation in the synthesized solids, a scanning electron microscope, FEI model Quanta 250 FP-2012/14 with tungsten filament, was used. The samples were coating with Au by the sputtering deposition method, using Quorum Q150R ES ionic coater.

XRD

Powder X-ray diffractograms were performed on the study samples in a SIEMENS D5005 diffractometer using Cu-Kα (λ=1.5456Å) radiation and Ni filter, in a range of 2θ: 20-80° with a step velocity of 0.04 °/s. Phase identification was realized using the JCPDS database.

The crystallite size (D_{hkl}) for the plane reflection of graphene oxide (001) was estimated using the Scherrer equation (equation 1). To simplify the calculation of the crystallite size, contributions from micro-deformations were assumed to be negligible, being expressed as:

$$D_{hkl} = \frac{K x \lambda}{\beta_{hkl} x \cos\theta} \qquad (1)$$

Where D_{hkl} corresponds to the average crystallite size in the normal direction of the family planes *hkl* = 001, K = 0.9 is the crystal shape factor, λ is the wavelength of the incident radiation (0.15418 nm), θ represents the position of the diffraction peak attributed to the plane of interest. β_{hkl} corresponds to the width at the medium height of the *hkl* reflection corrected for the instrumental broadening of the equipment. The values of β_{hkl} and θ were obtained by processing and analyzing the X-ray diffraction data with OriginPro 9.0 and converted to radians. The width at the medium height of the diffraction peak of the phase of interest (FWHM or β_o) in the samples was estimated by employing a Voigt nonlinear curve fitting function, which allowed the best fit to the experimental data. The instrumental broadening β_{inst} was corrected employing the equation 2 [11, 12].

$$\beta_{hkl} = \sqrt{(\beta_0 - \beta_{inst})\sqrt{(\beta_0{}^2 - \beta_{inst}{}^2)}} \qquad (2)$$

UV-Vis

The absorption spectra of GO3 in aqueous suspension (0.025 mg/mL) were measured in a Thermo Scientific Genesys 10S UV-Vis spectrophotometer.

RESULTS AND DISCUSSION

Preparation of GO and r-GO

In general, the preparation strategy of r-GO involved three steps (Fig. 1). 1) Graphite oxide was obtained by oxidation of powdered graphite dispersed in water, due to the presence of hydroxyl groups and epoxides in the basal plane of the graphite oxide and carboxyl groups at the edges [9]. 2) Graphite oxide was then exfoliated by ultrasound to form GO films. 3) GO was reduced by removing the oxygenated functional groups using *L*-ascorbic acid as a reducing agent.

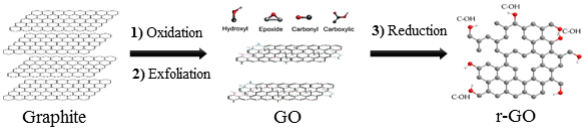

Fig 1. Steps in the synthesis of r-GO. Starting with the oxidation of graphite giving rise to graphite oxide, followed by its exfoliation to GO, which is reduced to obtain r-GO. Reproduced with permission from ref. [13].

In particular, the mechanism of formation of the oxidized materials (GO1 and GO3) was initiated by the addition of acids to the solid mixture of graphite and $KMnO_4$, giving rise to a dark green colored mixture with heat release. This coloration was indicative of the formation of Mn_2O_7, the active species responsible for oxidizing the graphite. This oxidizing agent is obtained by the reaction of monometallic tetroxide and MnO_3^+ (Fig. 2b) [14]. The transformation of $KMnO_4$ into a more reactive substance (Mn_2O_7), certainly helped to oxidize the graphite powder (Fig. 2c) [15].

$$KMnO_4 + 3\,H_2SO_4 \longrightarrow K^+ + MnO_3^+ + H_3O^+ + 3\,HSO_4^- \qquad (a)$$

$$MnO_3^+ + MnO_4^- \longrightarrow Mn_2O_7 \qquad (b)$$

$$Mn_2O_7 + H_2SO_4 + C(\text{grafito}) \longrightarrow MnO_5 + H_2O + \mathbf{GO}\begin{pmatrix}\text{C-O-C}\\ \text{C-OH}\\ \text{COOH}\end{pmatrix} + SO_4^{-2} \qquad (c)$$

Fig 2. Formation mechanism of GO [9].

As the reaction progressed, the dark green mixture (Fig. 3a) changed to a dark purple suspension (Fig. 3b), indicating that some of unreacted $KMnO_4$ remained. In turn, the addition of H_2O_2 to the mixture released heat and effervescence, producing a brown solution (Fig. 3c). The H_2O_2 was used to consume the residue $KMnO_4$ [9]. Different solvents were used in the washing processes of each of the graphitic oxides obtained. Particularly, in *Methodology 3*, the graphite oxide mass was treated with 30 % HCl solution to remove sulfate ions (SO_4^{2-}). During this process, a $BaCl_2$ solution was used as a screening test for SO_4^{2-}. A dark brown mass was obtained from these washes (Fig. 3d), and this was then dried to yield amorphous graphite oxide sheets (Fig. 3e). The pulverized material was successfully exfoliated by ultrasound treatment to obtain a brown solution of GO3 (Fig. 3f). The latter was possible thanks to the introduction of oxygenated functional groups, which provide the hydrophilic nature of this material [9, 16].

The reduction of GO3 with L-AA resulted in the solid r-GO3. This reaction was monitored by visual observation. The dark brown aqueous solution of GO3 (Fig. 3f), after reduction with *L*-AA resulted in a heterogeneous mixture, where a black colored solid was deposited at the bottom of the flask when stirring was stopped, resulting in r-GO3 (Fig. 3g). This was due to an increase in the hydrophobicity of the material, caused by a decrease in the oxygen-containing functional groups on the surface and edges of the films [17].

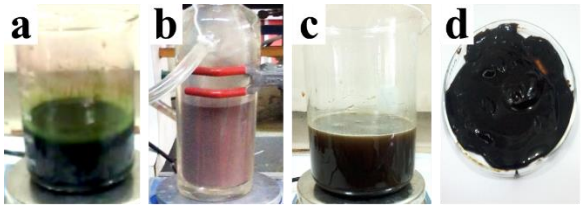

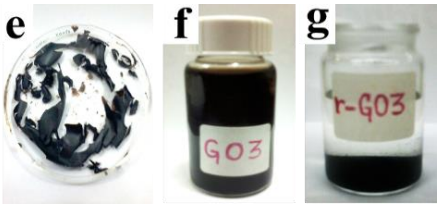

Fig. 3. Digital images taken during the different stages of the synthesis of r-GO3. (a) When the acid mixture is added to graphite and $KMnO_4$. (b) Dispersion obtained after 24 h of reaction. (c) After addition of H_2O_2. (d) Mass obtained after washing and centrifugation protocols. (e) Oven-dried graphite oxide sheets. (f) Aqueous suspension of ultrasound-exfoliated GO3. (g) Hydrophobic r-GO3 in DI water.

The mechanism of GO reduction by *L*-AA and the reason why it does not undergo complete reduction under moderate reaction conditions are not fully elucidated to date. Although, some authors have proposed that the five-membered ring of the *L*-AA molecule donates electrons to the GO, through a hydride transfer mechanism [10], opening the epoxide rings which become OH leaving groups, then *L*-AA donates a proton to the OH group, allowing the release of a water molecule to obtain a graphene sheet [9].

Characterization of GO and r-GO

N_2 physisorption

Figure 4a shows the adsorption-desorption isotherms of the synthesized materials GO1, GO2 and r-GO3. According to the IUPAC classification [18], their isotherms are of type II, corresponding to non-porous solids or macroporous adsorbents.

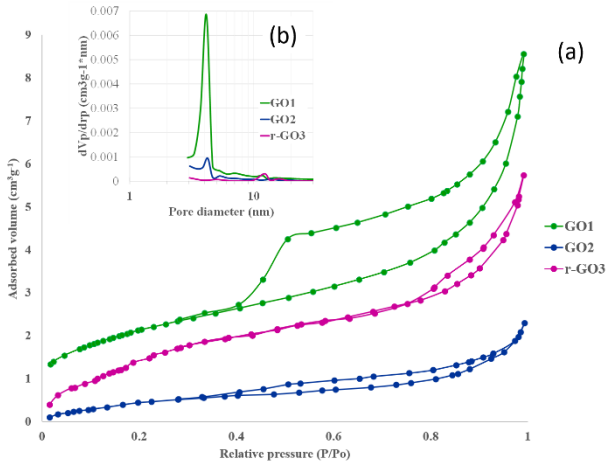

Fig. 4. Textural analysis of GO1, GO2 and r-GO3: (a) Nitrogen adsorption-desorption isotherm; (b) Pore size distribution.

The hysteresis loop observed in these materials can be classified as Type H3. These are related to solids consisting of aggregates or agglomerates of particles in the form of thin plates or sheets that form slit-like pores, with non-uniform size and shape [19-20].

In addition, the Figure 4b shows the pore size distribution for GO1, GO2 and r-GO3. For the first two oxides, the pore size value is centered in the range 3-5 nm. While for r-GO3 the pore size is mainly centered at 5 and 12.2 nm.

On the other hand, the GO3 solid exhibits a type IV isotherm (Fig. 5a), which is typical for adsorbent materials with a mesoporous structure and has also been observed in graphene-based materials reported in the literature [21]. In turn, the pore size distribution of GO3 showed a multimodal behavior, centered at 4.4, 6.9 and 10.3 nm, with different intensities in an increasing order with increasing pore size. This result is consistent with what is expected for a mesoporous type of material, with pore sizes between 2 and 50 nm according to IUPAC. It is also in line with reports of such graphene-derived materials [5, 18, 22]. It is worth noting that the BJH pore size distribution is mainly suitable for mesoporous solids due to its theoretical considerations [19]. But it is not so useful for the description of microporous and macroporous or non-porous solids. The latter being the porous system presented by GO1, GO2 and r-GO3. This explains the inconsistencies in the values of their size distribution found with the expected ranges according to the type of porous system of these materials.

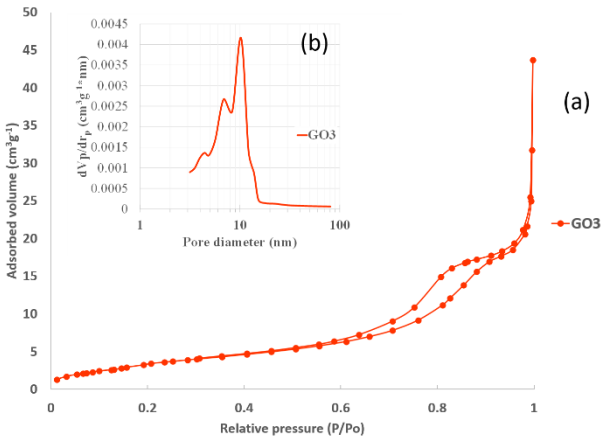

Fig. 5. Textural analysis of GO3: (a) Nitrogen adsorption-desorption isotherm; (b) Pore size distribution.

Table I shows the values of specific surface area (BET), total pore volume and average pore diameter for the graphene derivatives studied. These materials show relatively low values of surface area (2.1-14.2 m^2/g). However, GO1, GO2, GO3 exhibit surface areas in the range of values reported for graphene oxides obtained by Hummers [23] and even higher than GO obtained by a modified Hummers method (0.69 m^2/g) [24].

Table I. Textural characteristics of the materials.

Sample	$S_{g\ (BET)}$ (m^2/g)	V_p (cm^3/g)	D_p (nm)
GO1	7.8	0.0128	8.4
GO2	2.1	0.0037	7.3
GO3	14.2	0.0366	10.5
r-GO3	8.3	0.0073	6.5

$S_{g\ (BET)}$: Specific surface area (BET). V_p: Average pore volume. D_p: Average pore diameter.

However, the reduced derivative r-GO3 showed low S_g magnitudes compared to reduced graphene oxides using alcohols (5.8-35.9 m^2/g), ascorbic acid (122-403 m^2/g) and

hydrazine hydrate (80-500 m^2/g) as reducing agents [24, 25, 26]. In terms of total pore volume, the values were in the range of macroporous or nonporous type solids (GO1, GO2 and r-GO3). In particular, GO3 exhibited the largest total mesopore volume (0.04 cm^3/g) among the graphene derivatives synthesized in this study, which is at the lower limit of the range reported for graphene-based 3D porous materials (0.04-1.96 cm^3/g) [22, 23], consistent with its low specific surface area. The average pore diameter was in the range of 6.5-10.5 nm, which is classified as mesoporosity according to IUPAC. However, from the analysis of isotherms and other textural features considered above, only solid GO3 is attributed a mesoporous structure. The presence of mesopore range pores in GO1, GO2 and r-GO3 is not ruled out. Although it must be considered that these pores would be very superficial or shallow in relation to the internal surface of the solid. In coherence with the type of isotherm, low pore volume and low specific surface area presented.

UV-Vis

Figure 6 shows the UV-Vis spectra of an aqueous suspension of GO3. Two types of characteristic configurations can be observed in the spectra. The absorption peak at 228 nm corresponds to the $\pi \rightarrow \pi^*$ transitions of C=C bonds [8]. A broad band (shoulder) was also observed around 300 nm, which is attributed to the $n \rightarrow \pi^*$ transition of carbonyl groups (C=O). [8]. Similar UV-Vis spectra have been reported for graphene oxides synthesized from graphite [27, 28]. Thus, the formation of graphene oxide using the modified Hummers method presented in this study is confirmed.

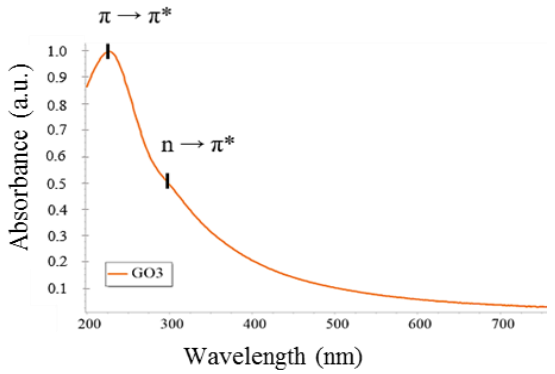

Fig. 6. UV-Vis absorption spectra of an aqueous suspension of GO3.

FT-IR

Infrared spectroscopy is a useful technique to characterize the presence of different functional groups in GO. The FT-IR spectra of the solids GO1, GO2 and GO3 confirmed the oxidation of the starting graphite (Fig. 7). Characteristic bands of functional groups such as O-H, COOH, C=C, C=O, C-OH and C-O were observed in these materials. Their IR spectra show a broad peak between 3650 cm^{-1} and 3000 cm^{-1}, corresponding to the O-H stretching (at 3420 cm^{-1}), which overlaps with the O-H stretching of the carboxylic acid and adsorbed water molecules. Two peaks at 2927 cm^{-1} and 2849 cm^{-1} correspond to the asymmetric and symmetric vibrations of CH_2 groups, respectively. The strong absorption band at 1630 cm^{-1} is attributed to the C=C stretching of the graphitic arrangement of unoxidized C-C sp^2 bonds [29]. The signal at 1720 cm^{-1} is attributed to the C=O stretching of the carbonyl group [9], and the peak at 1395 cm^{-1} is attributed to the bending vibrations of the O-H carboxyl bond [29]. The spectrum also shows bands at 1160 cm^{-1} and 1060 cm^{-1} assigned to the C-O stretching vibrations of the epoxy and alkoxy groups, respectively [30]. The presence of these oxygen-containing groups, especially the polar hydroxyl groups, favors the formation of hydrogen bonds with water molecules, which explains the hydrophilic nature of the synthesized GOs.

Respect to the infrared spectra of the reduced r-GO3 material, a decrease in the intensities of the peaks with

oxygen-containing functionalities was observed. For example, the intensity of the absorption band corresponding to the C=O group at 1720 cm^{-1} showed a decrease and a shift of the band profile at 1630 cm^{-1} (C=C, sp^2) appeared as a shoulder. In contrast to the other spectra of graphene oxides, in r-GO3 a new intense peak appears at 1575 cm^{-1}, corresponding to the skeleton vibrations (C=C) of graphene sheets [30-33]. This shows that GO3 was reduced. However, it is evident that not all of the peaks of oxygenated groups disappeared, indicating that the *L*-AA did not completely reduce the GO3. Another factor that possibly prevented a higher degree of reduction of this sample is attributed to the drying process, which was carried out at 100 °C in an air oven (oxidizing atmosphere).

XRD

Figure 8 shows the X-ray diffractograms of the graphene oxides GO1, GO2 and GO3, and the reduced graphene oxide r-GO3. The red dashed line located at 2θ = 26.4° corresponds to the reflection signal of the pristine graphite pattern of a hexagonal lattice in the plane (002) (JCPDS file 41-1487) with an interlayer spacing d=0.335 nm, representative of stacked graphene sheets in the graphitic structure [32].

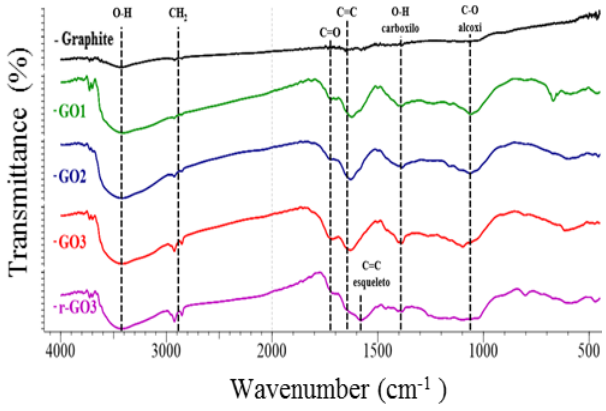

Figura 7. Espectros de FT-IR de los derivados de grafeno sintetizados y del grafito de partida.

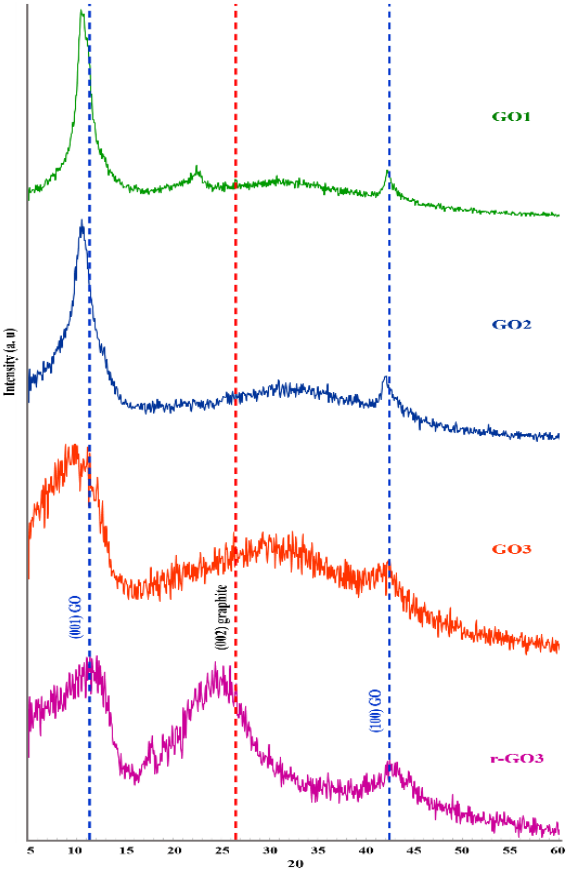

Fig. 8. X-ray diffractograms of GO1 (green line), GO2 (blue line), GO3 (orange line) and r-GO3 (purple line).

This signal was not very pronounced in GO1 and GO2, although in r-GO3 and to a lesser extent in GO3, it was observed overlapped by a broad band and with a significant lower angle shift in the reduced solid. This is attributed to the intercalation of water molecules and the formation of oxygen-containing functional groups between the graphite layers [32-34]. The amorphous form of this signal has been attributed to an amorphous carbon containing many defects and impurities that fold into sp^1, sp^2, and sp^3 hybridization structures [33]. It is worth mentioning that, in all materials, reflections at 2θ = 11.28° and 2θ = 42.38° attributed to graphene oxide were observed [32, 34-35]. Particularly, at the reflection 2θ = 11.28°, a shift was observed for all three graphene oxides, indicating possible structural defects in the sp^2 lattice of carbon.

Table I. Summary of interlayer distance and relative crystallite size in graphene derivatives

Material	$d_{001\text{-}GO}$ (nm)	$D_{001\text{-}GO}$ (nm)*
Grafito[1]	-	-
GO1	0.829	4.5
GO2	0.837	2.9
GO3	0.901	1.1
r-GO3	0.713	2.2

*: Obtained by Scherrer.
[1]: JCPDS file 41-1487.

Table I compares the interlayer spacing determined by Bragg in the (001) planes of graphene oxide "$d_{001\text{-}GO}$", which ranged between 0.83 and 0.90 nm, being slightly higher than those found in the literature [2-3]. This confirmed the oxidation of the starting graphite with the formation of graphene oxide, due to the introduction of oxygen-containing functional groups. On the other hand, a significant reduction of the interplanar spacing of r-GO3 (2θ = 24.3°) from 0.9 (GO3) to 0.7 nm could be appreciated, indicating the removal of oxygen-containing functional groups. However, the presence of the peak at $2\theta \approx 11.9°$ revealed certain domain of residual graphene oxide-type structure in this material, as evidenced by residual oxidized groups in the FT-IR spectrum for r-GO3. Similarly, Table I shows the average crystallite size calculated by Scherrer on the (001) plane signal corresponding to the main reflection of graphene oxide. A crystallite size value of less than 5 nm was found for the synthesized graphene derivatives, with a trend $D_{001\text{-}GO}$: GO3 < r-GO3 < GO2 < GO1. The reduction step applied to r-GO3 doubled the graphene oxide crystallite size with respect to the starting material (GO3), although it remained in the nanometer order.

SEM

The morphological analysis by SEM of graphene derivative systems in oxidized and reduced state is presented. In general, the synthesis protocols of the graphene derivatives presented in this study favored obtaining the carbon network in solid concretions with heterogeneous grain size in a relative size range approximately below 250µm (Fig. 9a-12a). The materials presented a common morphological characteristic, composed of aggregates of small thin sheets (<5µm), overlapping on each other forming layers and particular deformations. Being consistent with SEM results reported using similar synthesis methods [32, 34-35].

On the other hand, the GO1 solid showed concretions with a mostly flattened morphology with possible greater alignment of the constituent sheets of graphene oxide (Fig. 9), although not absent of deformations, being more evident at higher resolution (Fig. 9d). Similarly, GO2 showed flattened surfaces, but with a greater presence of disorder and defects in the sheet packing, which are more evident at higher resolution (Fig 10 b, c). Deformations of this type have been associated with the oxidation process of the graphene network [32, 35].

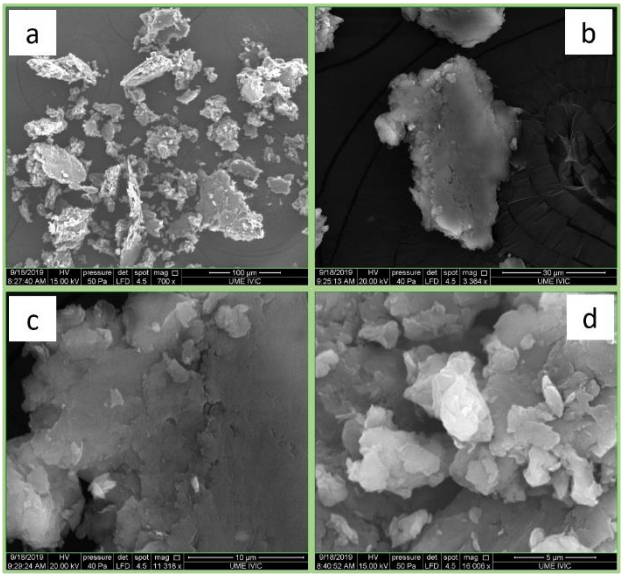

Fig. 9. SEM images of GO1 with magnification of a) 700x, b) 3364x, c) 11318x and d) 16006x.

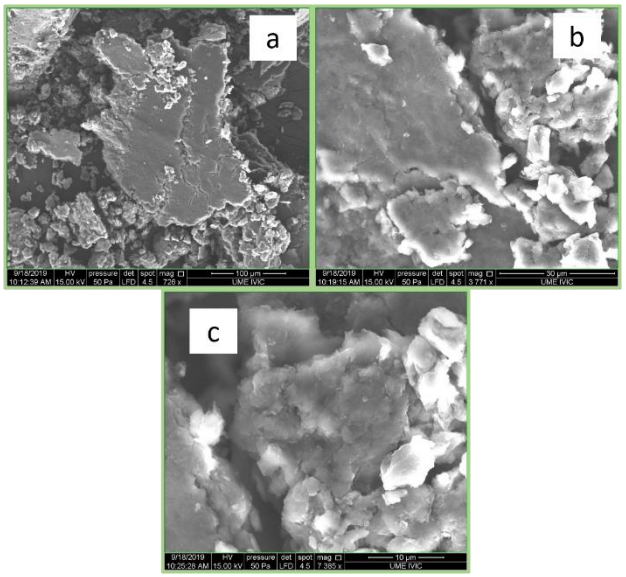

Fig. 10. SEM images of GO2 with magnification of a) 726x, b) 3771x y c) 7385x.

Continuing with the analysis, the GO3 solid showed the highest presence of interlayer roughness of graphene oxides, with a large presence of agglomerates of very small particles mainly at the edges of the concretion (Fig. 11 c-d). This would be associated with the significant incorporation of oxidized functional groups in the basal lattice of graphene [34-35]. The GO3 graphene oxide exhibited a rougher morphology, with fissures and defective zones of the submicrometric order, which could be useful for the possible incorporation of chemical species as active sites of interest in catalysis. Such results are in agreement with XRD, FTIR, UV-VIS and textural analysis. Finally, in the SEM analysis of the reduced graphene derivative r-GO3 (Fig. 12a), a significant decrease in concretion size (<50μm) was observed compared to the oxidized graphene derivatives. However, it showed a less rough morphology than its precursor GO3, a dense irregular stacking of sheets, with wavy and flexible edges. Similar observations have been reported in r-GO obtained by modified Hummers methods and thermally reduced using malonic acid. [35].

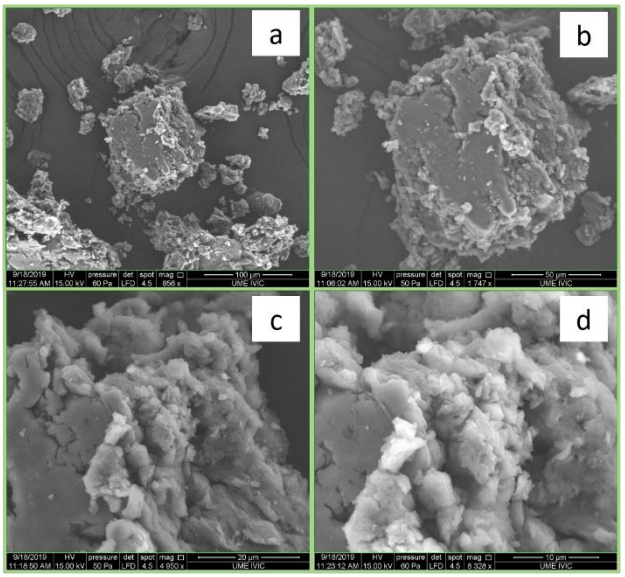

Fig. 11. SEM images of GO3 with magnification of a) 856x, b) 1747x, c) 4950x y d) 8328x.

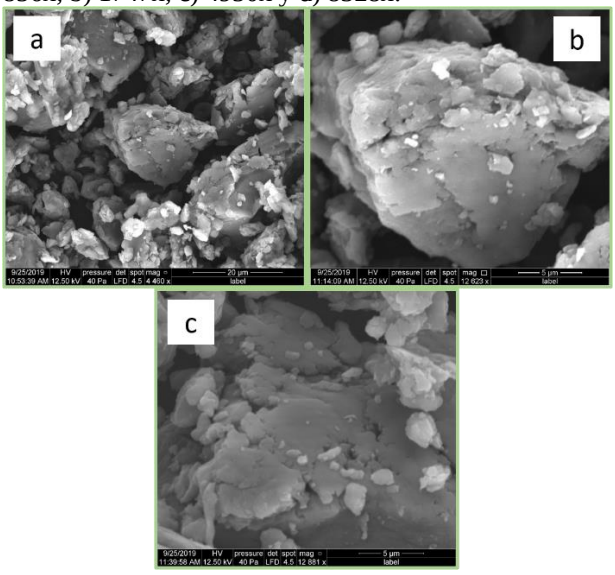

Fig. 12. SEM images of r-GO3 with magnification of a) 4460x, b) 12623x y c) 12881x.

This result is in agreement with what was revealed by XRD and FT-IR analysis for the r-GO solid, in terms of the decrease in interlayer spacing due to the removal of oxidized groups up to a certain extent of the material. It is also consistent with the textural analysis, which showed a change in the porous texture due to the reduction of GO3, going from a mesoporous solid to a macro- or non-porous one, with loss of specific surface area and pore volume. Likewise, the densification of the interlaminar stacking is consistent with the increase in crystallite size relative to

the (001) plane of graphene oxide when going from GO3 to r-GO3. Although with a slow stacked growth to a narrower range of confinement or extension of concretion, with respect to the other solids. In this sense, Popov et al reported SEM results at a higher resolution (micro-mark between 1-2μm) for r-GO obtained from a modified Hummers synthesis and using malonic acid as a reducing agent [32] [32]. In addition to the particular considerations of the study, the morphological structure of r-GO was described as an irregular stacking of graphene layers that were torn, giving rise to the formation of veil-shaped sheets with wavy edges [32].

In summary, when comparing the different carbonaceous materials in the present study, graphene oxide GO3 obtained by modified Hummers methodology, proved to be the only mesoporous solid, with the highest degree of oxygenated group intercalation and with more promising textural, structural and morphological properties for its application as a catalytic support. In turn, the textural and morphological features and the possible presence of defect sites in the graphene lattice, which involve the corresponding partial restoration of the π-conjugated sp^2 carbon structure, the latter reported to improve the electrical conductivity of r-GO [32, 36], make this material interesting for applications as biosensor electrodes [37]. Promising electromagnetic properties have also been reported for r-GO as a microwave absorber [38].

CONCLUSIONS

In this study, three experimental protocols were applied to synthesize graphene oxide solids (GO1, GO2 and GO3) under Hummers and modified Hummers methodologies. Then, GO3 was reduced with *L*-AA as an eco-friendly strategy to obtain r-GO3. The average crystallite size calculated by Scherrer was less than 5 nm for the synthesized graphene derivatives, in the order: GO3 < r-GO3 < GO2 < GO1. The GO solids presented in general, a morphology conformed by aggregates of small thin sheets, overlapping on each other forming layers and particular deformations, defects and roughness in the layer edges, in lesser (r-GO3 case) or greater degree (GO3 case), attributed to the process of incorporation of oxygenated functional groups to the graphene carbon network. This correlated with an increase in the interlayer spacing in the (001) d_{001} planes of GO, confirming the oxidation of the starting graphite to graphene oxide by the introduction of oxygenated functional groups into the basal network of graphene. As well as, to the formation of a characteristic porous structure being of the mesoporous type for GO3 and macroporous or non-porous for the GO1, GO2 and r-GO3 derivatives.

In relation to r-GO, the decrease in the interlayer spacing of the (001) d_{001} planes of GO was associated with the removal of oxidized groups, the restoration of the domain associated with the graphene structure and the residual GO structure, causing a transformation to macro- or non-porosity with lower surface area and pore volume compared to its precursor GO3.

When comparing the different carbonaceous materials of the present study, the graphene oxide GO3, obtained by a proposed modified Hummers method, turned out to be the only mesoporous solid, with the highest degree of intercalation of oxygenated groups and with more promising textural, structural and morphological properties for its application as a catalytic support. The r-GO solid, on the other hand, may be more interesting for applications independent of its surface and porosity, such as electrical conductivity and electromagnetic properties, among others.

ACKNOWLEDGEMENT

The authors thank to the Electron Microscopy Unit (UME) of the Center for Chemistry, IVIC and Eng. Jeanhiasary Anzola, for carrying out the SEM analysis. We also thank to BS. Liz Cubillán of the Applied Chemistry Laboratory for her support in the FT-IR analysis.

REFERENCES

[1] Dreyer D.R., Ruoff R.S., Bielawski C.W. (2010) "From conception to realization: an historical account of graphene and some perspectives for its future" *Angew. Chem. Int. Ed.* 49:9336-9344.

[2] Hummers W.S., Offeman R.E. (1958) "Preparation of graphitic oxide" *J. Am. Chem. Soc.* 80:1339-1339.

[3] Feicht P., Biskupek J., Gorelik T.E., Renner J., Halbig C.E., Maranska M., Puchtler F., Kaiser U., Eigler S. (2019) "Brodie's or Hummers method: oxidation conditions determine the structure of graphene oxide" *Chem. Eur. J.* 25: 8955-8959.

[4] Viprya P., Kumar D., Kowshik S. (2023) "Study of different properties of graphene oxide (GO) and Reduced Graphene Oxide (rGO)" *Eng. Proc.* 59:84.

[5] Wei Z., Guo D., Hou Y., Xu H., Liu Y. (2016) "Progress on the graphene-involved catalytic hydrogenation reactions" *J. Taiw. Inst. Chem. Eng.* 67:126-139.

[6] Furst A., Berlo R.C., Hooton S. (1965) "Hydrazine as a reducing agent for organic compounds (catalytic hydrazine reductions)" *Chem. Rev.* 65:51–68.

[7] Zhang J., Yang H., Shen G., Cheng P., Zhang J., Guo S. (2010) "Reduction of graphene oxide vial-ascorbic acid" *Chem. Commun.* 46:1112–1114.

[8] Ranjan P., Agrawal S., Sinha A., Rao T.R., Balakrishnan J., Thakur A.D. (2018) "A low-cost non-explosive synthesis of graphene oxide for scalable applications" *Sci. Rep.* 8:1-13.

[9] Emiru T.F. and Ayele D.W. (2016) "Controlled synthesis, characterization and reduction of graphene oxide: A convenient method for large scale production" *Egypt. J. Bas. Appl. Sci.* 4:74-79.

[10] Fernández M.J., Guardia L., Paredes J.I., Villar S., Solís P., Martínez A., Tascón J.M.D. (2010) "Vitamin C is an ideal substitute for hydrazine in the reduction of graphene oxide suspensions" *J. Phys. Chem. C* 114:6426-6432.

[11] Suryanarayana C. and Norton M.G. (1998) "*X-Ray Diffraction A Practical Approach*" New York, Springer Science+Business Media, pp. 207-221.

[12] Shafi P.M. and Bose A.C. (2015) "Impact of crystalline defects and size on X-ray line broadening: A phenomenological approach for tetragonal SnO_2 nanocrystals" *AIP Adv.* 5:057137.

[13] Bonaccorso F., Lombardo A., Hasan T., Sun Z., Colombo L., Ferrari A.C. (2012) "Production and processing of graphene and 2d crystals" *Mater. Today* 15:564-589.

[14] Koch K.R. "Oxidation by Mn_2O_7: An impressive demonstration of the powerful oxidizing property of dimanganese heptoxide" J. Chem. Educ. 59 (1982) 973.

[15] Allahbakhsh A., Sharif F., Mazinani S., Kalaee M.R. (2014) "Synthesis and characterization of graphene oxide in suspension and powder forms by chemical exfoliation method" *Int. J. Nano. Dimens.* 5:11–20.

[16] Zhang T.Y., Zhang D. (2011) "Aqueous colloids of graphene oxide nanosheets by exfoliation of graphite oxide without ultrasonication" *Bull. Mater. Sci.* 34:25–28

[17] Stankovich S., Dikin D.A., Piner R.D., Kohlhaas K.A., Kleinhammes A., Jia Y., Wu Y., Nguyen S.T., Ruoff R.S. (2007) "Synthesis of graphene-based nanosheets via chemical reduction of exfoliated graphite oxide" *Carbon* 45:1558–1565.

[18] Rouquerol F., Rouquerol J., Sing K., Llewellyn P., Maurin G. (2014) "*Adsorption by Powders and Porous Solids*" Elsevier, second edition, Oxford, UK.

[19] Sing K., Everett D., Haul R., Moscou L., Pierotti R., Rouquerol J., Siemieniewska T. (1985) "Reporting physisorption data for gas/solid systems with special reference to the determination of Surface Area and Porosity" *Pure Appl Chem 57: 603-619.*

[20] Leofanti G., Padovan M., Tozzola G., Venturelli B. (1998) "Surface area and pore texture of catalysts" *Catal. Today* 41: 207-219

[21] Li Z.F., Zhang H., Liu Q., Sun L., Stanciu L., Xie J. (2013) "Fabrication of high-surface-area graphene/polyaniline nanocomposites and their application in supercapacitors" *ACS Appl. Mater. Interfaces* 5: 2685-2691.

[22] L. Zhang, F. Zhang, X. Yang, G. Long, Y. Wu, T. Zhang, K. Leng, Y. Huang, Y. Ma, A. Yu, Chen Y. (2013) "Porous 3D graphene-based bulk materials with exceptional high surface area and excellent conductivity for supercapacitors" *Sci. Rep.* 3:1408.

[23] Alam S.N., Sharma N., Kumar L. (2017) "Synthesis of graphene oxide (GO) by Modified Hummers method and its thermal reduction to obtain reduced graphene oxide (rGO)" *Graphene* 6: 1-18.

[24] Dreyer D.R., Murali S., Zhu Y., Ruoff R.S. y Bielawski C.W. (2011) "Electronic supporting information reduction of graphite oxide using alcohols" *J. Mat. Chem.* 21: 3443-3447.

25 Park S., An J., Potts J.R., Velamakanni A., Murali S., Ruoff R.S. (2011) "Hydrazine-reduction of graphite- and graphene oxide" *Carbon* 49: 3019-3023.

26 Ortiz-Anaya I., Nishina Y. (2023) "Unveiling the reduction process of graphene oxide by ascorbic acid: grafting and reduction sequences for high surface area graphene materials" *Chem plus chem.* 88 (8): e202300328.

27 Luo Z, Lu Y, Somers L.A, Johnson A.T.C. (2009) "High yield preparation of macroscopic graphene oxide membranes" *J. Am. Chem. Soc*. 131: 898-899.

28 Chen D., Li L., Guo L. (2011) "An environment-friendly preparation of reduced graphene oxide nanosheets via amino acid" *Nanotechnology* 22:325601.

[29] Guo H.L., Wang X.F., Qian Q.Y., Wang F.B., Xia X.H. (2009) "A green approach to the synthesis of graphene nanosheets" *ACS Nano* 3:2653–2659

[30] Murugan, A.V., Muraliganth, T. and Manthiram, A., (2009) "Rapid, facile microwave-solvothermal synthesis of graphene nanosheets and their polyaniline nanocomposites for energy storage" *Chem. Mat.* 21: 5004-5006.

[31] Xu C., Yuan R.S., Wang X. (2014) "Selective reduction of graphene oxide" *New Carbon Mater.* 29: 61–66.

32: Popov A., Aukstakojyte R., Gaidukevic J., Lisyte V., Kausaite-Minkstimiene A., Barkauskas J., Ramanaviciene A. (2021) "Reduced graphene oxide and polyaniline nanofibers nanocomposite for the development of an amperometric glucose biosensor" *Sensors* 21: 948

33: Huh S.H. (2011) "Thermal Reduction of Graphene Oxide" in *Physics and Applications of Graphene – Experiments,* S. Mikhailov (Ed.), Croatia, InTech Europe, p. 73.

34: Shalaby A., Nihtianova D., Markov P., Staneva A.D., Iordanova R. S., Dimitriev Y. B., (2015) "Structural analysis of reduced graphene oxide by transmission electron microscopy" *Bulg. Chem. Commun.* 47: 291–295.

35: Bhattacharyya S., Banerjee P., Bhattacharya S., Singh Rathour R.K., Majumder S.K., Das P., Datta S., (2018) "Comparative assessment on the removal of ranitidine and prednisolone present in solution using graphene oxide (GO) nanoplatelets" *Desalin Water Treat* 132: 287–296.

36 Rao, S., Upadhyay, J., Polychronopoulou, K., Umer, R., Das, R. (2018) "Reduced graphene oxide: effect of reduction on electrical conductivity" *J. Compos. Sci.*, 2: 25.

37 Tite, T., Chiticaru, E.A., Burns, J.S., Ionita, M, J. (2019) "Impact of nano-morphology, lattice defects and conductivity on the performance of graphene based electrochemical biosensors" *Nanobiotechnology* 17: 101.

38 Wang C., Han X., Xu P., Zhang X., Du Y., Hu S., Wang J., Wang X. (2011) "The electromagnetic property of chemically reduced graphene oxide and its

application as microwave absorbing material" *Appl. Phys. Lett*. 98: 072906.